Biochemical and Structural Studies with Prenyl Diphosphate Analogues Provide Insights into Isoprenoid Recognition by Protein Farnesyl Transferase[†,‡]

Tammy C. Turek-Etienne,[§] Corey L. Strickland,[||] and Mark D. Distefano*[,§]

Department of Chemistry, University of Minnesota, Minneapolis, Minnesota 55455, and Department of Structural Chemistry, Schering-Plough Research Institute, Kenilworth, New Jersey 07033

Received August 20, 2002; Revised Manuscript Received January 8, 2003

ABSTRACT: Protein farnesyl transferase (PFTase) catalyzes the reaction between farnesyl diphosphate and a protein substrate to form a thioether-linked prenylated protein. The fact that many prenylated proteins are involved in signaling processes has generated considerable interest in protein prenyl transferases as possible anticancer targets. While considerable progress has been made in understanding how prenyl transferases distinguish between related target proteins, the rules for isoprenoid discrimination by these enzymes are less well understood. To clarify how PFTase discriminates between FPP and larger prenyl diphosphates, we have examined the interactions between the enzyme and several isoprenoid analogues, GGPP, and the farnesylated peptide product using a combination of biochemical and structural methods. Two photoactive isoprenoid analogues were shown to inhibit yeast PFTase with K_I values as low as 45 nM. Crystallographic analysis of one of these analogues bound to PFTase reveals that the diphosphate moiety and the two isoprene units bind in the same positions occupied by the corresponding atoms in FPP when bound to PFTase. However, the benzophenone group protrudes into the acceptor protein binding site and prevents the binding of the second (protein) substrate. Crystallographic analysis of geranylgeranyl diphosphate bound to PFTase shows that the terminal two isoprene units and diphosphate group of the molecule map to the corresponding atoms in FPP; however, the first and second isoprene units bulge away from the acceptor protein binding site. Comparison of the GGPP binding mode with the binding of the farnesylated peptide product suggests that the bulkier isoprenoid cannot rearrange to convert to product without unfavorable steric interactions with the acceptor protein. Taken together, these data do not support the "molecular ruler hypotheses". Instead, we propose a "second site exclusion model" in which PFTase binds larger isoprenoids in a fashion that prevents the subsequent productive binding of the acceptor protein or its conversion to product.

Protein farnesyl transferase (PFTase)[1] catalyzes the reaction between farnesyl diphosphate (**1**) and a protein substrate to form a thioether-linked prenylated protein (*1*−*5*). Related protein geranylgeranyl transferases (PGGTase) act on a C_{20} homologue, geranylgeranyl diphosphate (**2**), to transfer this longer isoprenoid group to a different set of proteins (*6*). These reactions are summarized in Figure 1. Protein prenylation is a ubiquitous posttranslational modification since virtually all small monomeric GTP binding proteins, the γ-subunits from heterotrimeric G-proteins, and many other proteins are so modified (*7*, *8*). The fact that many prenylated proteins are involved in signaling processes has generated considerable interest. In particular, the observation that Ras proteins are farnesylated and that the inhibition of prenylation of oncogenic Ras variants halts the growth of certain types of cancer has sparked an explosion of work in this area (*9*−*13*). Several pharmaceutical companies now have inhibitors of PFTase in phase II clinical trials which show promise for cancer treatment (*14*−*18*). Inhibitors of PGGTase I are also being explored as possible anticancer agents (*19*).

In an effort to design inhibitors that are specific for their cognate protein prenyl transferase, considerable effort has been focused on understanding the underlying basis for the substrate specificity of these enzymes. While the protein targets of PFTase and PGGTase I are largely defined by the identity of the C-terminal residue and to a lesser extent other residues in the CAAX recognition box (*20*), the rules for isoprenoid recognition for these enzymes are less well understood. In the case of PFTase, it has been known that despite the fact that this enzyme manifests substantial affinity for GGPP, that isoprenoid is not efficiently utilized by the enzyme as a substrate (*21*, *22*). A considerable amount of structural data obtained via X-ray crystallographic studies

[†] This work was supported by NIH Grant GM58842.

[‡] The atomic coordinates and structure factors (codes 1o1s, 1o1r, and 1o1t for PFTase bound with **3b**, GGPP, and the farnesylated product, respectively) have been deposited in the Protein Data Bank, Research Collaboratory for Structural Bioinformatics, Rutgers University, New Brunswick, NJ (http://www.rcsb.org/).

* To whom correspondence should be addressed. Phone: (612) 624-0544. Fax: (612) 626-7541. E-mail: distefan@chem.umn.edu.

[§] University of Minnesota.

[||] Schering-Plough Research Institute.

[1] Abbreviations: PFTase, protein farnesyl transferase; PGGTase, protein geranylgeranyl transferase; FPP, farnesyl diphosphate; GGPP, geranylgeranyl diphosphate; DTT, dithiothreitol; TLC, thin-layer chromatography; EDTA, ethylenediaminetetraacetic acid; SDS−PAGE, sodium dodecyl sulfate−polyacrylamide gel electrophoresis; HPLC, high-performance liquid chromatography; ESI-MS, electrospray ionization mass spectrometry; BSA, bovine serum albumin.

10.1021/bi0266838 CCC: $25.00
Published on Web 03/15/2003

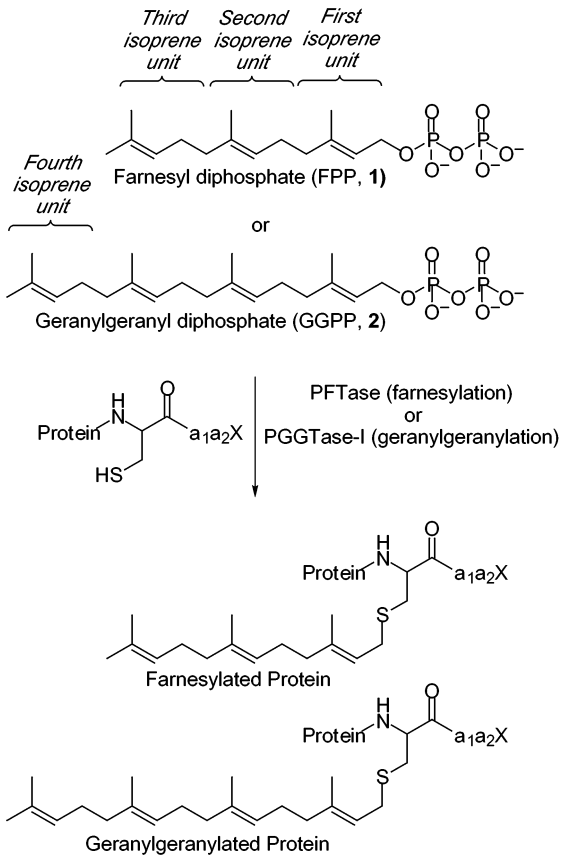

FIGURE 1: Reaction catalyzed by PFTase and PGGTase I.

is now available for PFTase (*23*−*30*). On the basis of early work with the FPP•PFTase binary complex structure, Beese and co-workers advanced the molecular ruler hypothesis in which the prenyl diphosphate specificity is governed by the depth of the isoprenoid binding pocket in PFTase. In particular, they suggested that PFTase binds to GGPP in a conformation where C-1 of the allylic diphosphate is not correctly positioned for efficient attack by the protein-derived Zn(II)−thiolate nucleophile (*24*). To clarify how PFTase discriminates between FPP and larger prenyl diphosphates, we have examined the interactions between the enzyme and GGPP, several isoprenoid analogues shown in Figure 2, and a farnesylated peptide using a combination of biochemical and structural methods. These studies suggest an alternative explanation for how PFTase is able to differentiate between FPP and GGPP.

MATERIALS AND METHODS

Materials. UV spectra were obtained using a Hewlett-Packard 8452A spectrophotometer, and fluorescence measurements were performed with a Perkin-Elmer LS 50B luminescence spectrometer. HPLC analysis was carried out using a Beckman Model 127/168 instrument equipped with a diode array UV detector and a Beckman 6300A fluorescence detector (305−395 nm excitation filter and 480−520 nm emission filter). Preparative HPLC separations were performed with a Rainin Dynamax Microsorb C_{18} column (2.14 × 25 cm with a 5 cm guard column), while analytical HPLC separations employed a Rainin Dynamax Microsorb C_{18} column (5 μm, 4.6 × 250 mm) or a Vydac C_{18} column (5 μm, 4.6 × 250 mm). Phosphorimaging analysis was performed with a Molecular Dynamics 445 SI phosphorimager. Dowex 50W-X8 resin and the silver staining kit were obtained from Bio-Rad, and Sep-Pak columns were purchased from Waters. [^{32}P]H_3PO_4 (specific activity 8500−9120 Ci/mmol) was obtained from DuPont NEN. NaB^3H_4 (specific activity 15 Ci/mmol) was purchased from American Radiolabeled Chemicals, Inc. *N*-Ds-GCVIA was purchased from Bio-synthesis, Inc. *N*-Dansylglycine was obtained from Sigma. TFA was purchased from Fisher, and liquid scintillation fluid was purchased from Cytoscint. *Escherichia coli* DH5α/pGP114 was a generous gift from C. D. Poulter, Department of Chemistry, University of Utah. Purified human PFTase was a generous gift from C. A. Omer, Merck Research Laboratories. ESI-MS/MS was performed by Dr. Leo Bonilla and Nancy Raha, University of Minnesota Cancer Institute. Compounds **3a** and **3b** and their corresponding alcohol and bromide precursors were prepared as previously described (*31*).

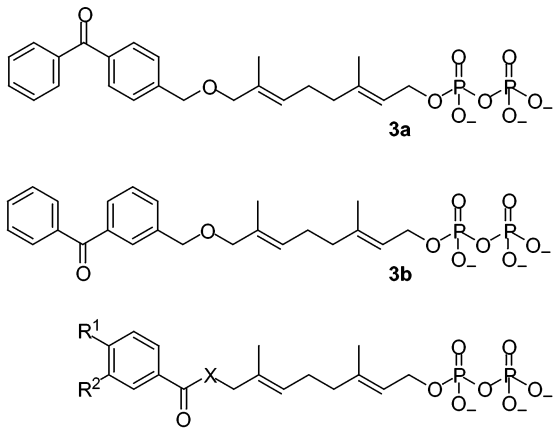

3c (R^1 = C_6H_5CO, R^2 = H, X = O)
3d (R^1 = H, R^2 = C_6H_5CO, X = O)
3e (R^1 = H, R^2 = C_6H_5CO, X = NH)

FIGURE 2: Prenyl diphosphate analogues employed in this study.

*N-Ds-GC(4-BBG)VIA (**4a**) and N-Ds-GC(3-BBG)VIA (**4b**).* Compound **4a** or **4b** was prepared by reacting the corresponding isoprenyl bromides with *N*-dansyl-GCVIA under acidic conditions containing DMF/butanol/0.025% TFA (2:1:1 v/v/v) and 1.0 M $Zn(OAc)_2$ as a catalyst as described by Xue et al. (*32*). The crude product was purified by reversed-phase HPLC employing a H_2O/CH_3CN (containing 0.2% TFA) gradient. The sample was collected, concentrated, and analyzed by ESI-MS and ESI-MS/MS. ESI-MS for **4a**: $C_{55}H_{73}O_{10}N_6S_2$ $[M + H]^+$, calcd 1041.5, found 1041.2; $C_{55}H_{72}O_{10}N_6S_2Na$ $[M + Na]^+$, calcd 1063.5, found 1063.2; $C_{55}H_{72}O_{10}N_6S_2K$ $[M + K]^+$, calcd 1079.5, found 1079.2. ESI-MS for **4b**: $C_{55}H_{73}O_{10}N_6S_2$ $[M + H]^+$, calcd 1041.5, found 1041.2; $C_{55}H_{72}O_{10}N_6S_2Na$ $[M + Na]^+$, calcd 1063.5, found 1063.2; $C_{55}H_{72}O_{10}N_6S_2K$ $[M + K]^+$, calcd 1079.5, found 1079.2. **4a**: UV (H_2O/CH_3CN/TFA, 50/50/0.2) λ_{max} = 320 nm, ϵ = 1780 $M^{-1}\cdot cm^{-1}$; fluorescence (H_2O/CH_3CN/TFA, 50/50/0.2) λ_{ex} = 322 nm, λ_{em} = 530 nm, intensity = 0.31 (relative to *N*-dansylglycine, 1.0). **4b**: UV (H_2O/CH_3CN/TFA, 50/50/0.2) λ_{max} = 320 nm, ϵ = 1780 $M^{-1}\cdot cm^{-1}$; fluorescence (H_2O/CH_3CN/TFA, 50/50/0.2) λ_{ex} = 322 nm, λ_{em} = 530 nm, intensity = 0.41 (relative to *N*-dansylglycine, 1.0).

*(E,E)-[α,β(n)-^{32}P]-8-O-(4-Benzoylbenzyl)-3,7-dimethyl-2,6-octadiene 1-Diphosphate ([^{32}P]-**3a**).* The alcohol precursor to **3a** was pyrophosphorylated with [^{32}P]H_3PO_4 and CCl_3CN and the product purified on a Sep-Pac reversed-phase C_{18} column using a stepwise gradient of CH_3CN and NH_4HCO_3 as previously described (*33*). The product [^{32}P]-**3a** eluted at 35% CH_3CN giving a 0.7% yield (specific activity 2100 Ci/mol). The concentration was determined by UV using the λ and ϵ for **3a**. The radiochemical purity was assessed by TLC (*i*-PrOH/NH_4OH/H_2O, 6:3:1 v/v/v) followed by phosphorimaging analysis giving 45% diphosphate. The corresponding monophosphate was the other major constituent.

*(E,E)-[α,β(n)-^{32}P]-8-O-(3-Benzoylbenzyl)-3,7-dimethyl-2,6-octadiene 1-Diphosphate ([^{32}P]-**3b**).* Compound [^{32}P]-**3b** was prepared as described above for [^{32}P]-**3a**. After reversed-phase chromatography, [^{32}P]-**3b** eluted at 30% and 35% CH_3CN, giving a 1.3% yield (specific activity 2800 Ci/mol) and 44% radiochemical purity.

Substrate Studies. Large-scale reactions contained 50 mM Tris·HCl, pH 7.0, 10 mM $MgCl_2$, 10 μM $ZnCl_2$, 5.0 mM DTT, 2.4 μM *N*-Ds-GCVIA, 45 nM yPFTase, and FPP (10 μM), **3a** (10 μM), or **3b** (10 μM), where appropriate, in a final reaction volume of 10 mL. The reactions were equilibrated to 30 °C, initiated by the addition of yPFTase, and allowed to react for 1 h. To desalt the samples, each reaction mixture was applied to a Sep-Pak C_{18} cartridge, washed with H_2O/CH_3CN/TFA (95:5:0.1 v/v/v), eluted with CH_3CN/TFA (100:0.1 v/v), concentrated in vacuo, dissolved in H_2O/CH_3CN/TFA (50:50:0.2 v/v/v), and analyzed by HPLC using a C_{18} reversed-phase column and a H_2O/CH_3CN/TFA gradient.

Enzyme Inhibition. IC_{50} values were determined for **3a** and **3b** with yPFTase by running duplicate assays with FPP and *N*-Ds-GCVIA maintained at 2 μM and **3a** at concentrations of 0, 0.30, 0.50, 1.0, 3.0, and 5.0 μM or **3b** at concentrations of 0, 0.16, 0.32, 0.50, 1.0, and 5.0 μM. An enzyme concentration of 5.0 nM yPFTase was employed. By plotting $1/v$ versus the inhibitor concentration (*34*), the rates were calculated. With these values known, competitive inhibition studies were performed using a 4 × 6 grid of duplicate assays with FPP maintained at fixed concentrations (1.0, 1.5, 3.0, and 7.0 μM) and varying concentrations of **3a** and **3b** at each concentration of natural substrate for yPFTase. Concentrations of 0, 0.20, 0.40, 0.80, and 1.6 μM for **3a** with yPFTase and 0, 0.15, 0.30, 0.60, and 0.90 μM for **3b** with yPFTase were chosen on the basis of the above IC_{50} values. In these experiments, the concentration of yPFTase was 2.5 nM, and the concentration of *N*-Ds-GCVIA was fixed at 2.4 μM. The rates were determined from the initial velocity measurements and K_I values calculated from Eadie−Hofstee plots.

Photoinactivation Studies. Photolysis reactions were conducted at 4 °C in a UV Rayonet mini-reactor equipped with eight RPR-3500 Å lamps and a circulating platform that allows up to eight samples to be irradiated simultaneously. All reactions (0.50−1.0 mL) were performed in silinized quartz test tubes (10 × 75 mm) and contained 52 mM Tris·HCl, pH 7.0, 5.8 mM DTT, 12 mM $MgCl_2$, 12 μM $ZnCl_2$, 25 mM NH_4HCO_3, and 38 nM yPFTase. Where appropriate, reactions contained **3a** (0.45 μM) or **3b** (0.49 μM); these concentrations were chosen to be 10 times above their calculated K_I values. For substrate protection experiments, FPP was added to a final concentration of 100 μM. Reactions were photolyzed for up to 12 h during which time duplicate samples (50 μL) were removed at various intervals, placed on ice, and assayed for activity.

*Photolabeling Reactions of yPFTase and hPFTase with [^{32}P]-**3a** and [^{32}P]-**3b**.* All reactions (100 μL) were performed in silinized quartz test tubes (10 × 75 mm) and contained 52 mM Tris·HCl, pH 7.0, 5.8 mM DTT, 12 mM $MgCl_2$, 12 μM $ZnCl_2$, 25 mM NH_4HCO_3, and 380 nM yPFTase (2.9 μg). Each reaction contained [^{32}P]-**3a** (9.1 μM) or [^{32}P]-**3b** (3.8 μM). The values used for the analogues with yPFTase were 10-fold above the K_I values obtained from experiments described above. For substrate protection experiments, FPP was added to a final concentration of 100 μM. Reactions were photolyzed for 2 h using the apparatus described above. Loading buffer [50 μL; 4% SDS, 12% glycerol (w/v), 50 mM Tris·HCl, 2% mercaptoethanol (v/v), 0.01% bromophenol blue] was then added to each sample, and the samples were heated to 70 °C for 5−10 min followed by analysis by SDS−polyacrylamide gel electrophoresis with a 10% Tris-Tricine gel. Gels were silver stained, dried, and subjected to autoradiography at −80 °C with an intensifying screen for 6−24 h for yPFTase or were exposed to a phosphorimaging screen for 24 h. The relative intensities of photolabeled products were determined by phosphorimaging analysis of the dried gels. Similar experiments were perfomed using hPFTase (390 nM).

X-ray Crystallographic Studies. Recombinant rPFTase was used for all structural studies and was prepared as previously reported (*27*). Crystals of the PFTase·**3b** and PFTase·GGPP complexes were prepared by soaking **3b** or GGPP into preformed crystals using methods previously described (*27*). X-ray diffraction data for the PFTase·**3b** complex were collected on a Rigaku rotating anode generator equipped with osmic mirrors and a Raxis-IV image plate detector. With the detector set at 135 mm, data were collected in 192 contiguous 0.30° oscillation images each exposed for 12 min. The data extend to 2.3 Å resolution and have an R_{merge} of 3.8% with a 3.4-fold multiplicity. The structure was refined using X-PLOR98.1 (Molecular Simulations Inc.) to an R_{factor} of 19.0%. X-ray diffraction data for the PFTase·GGPP complex were collected on the IMCA 17-ID beamline at the APS and a MAR165 CCD detector. With the detector set at 150 mm and using 1.0 Å wavelength X-rays, data were collected in 200 contiguous 0.30° oscillation images each exposed for 10 s. The data extend to 2.3 Å resolution and have an R_{merge} of 6.3% with a 3.7-fold multiplicity. The structure was refined using X-PLOR98.1 (Molecular Simulations Inc.) to an R_{factor} of 17.7%. Cocrystals of the PFTase·CVIM-farnesyl complex were prepared using methods previously described (*27*). X-ray diffraction data for the PFTase·CVIM-farnesyl complex were collected on a Rigaku rotating anode generator equipped with MSC Yale style mirrors and a Raxis-IV image plate detector. With the detector set at 135 mm, data were collected in 131 contiguous 0.30° oscillation images each exposed for 12 min. The data extend to 2.1 Å resolution and have an R_{merge} of 4.0% with a 2.5-fold multiplicity. The structure was refined using X-PLOR98.1 (Molecular Simulations Inc.) to an R_{factor} of 19.8%.

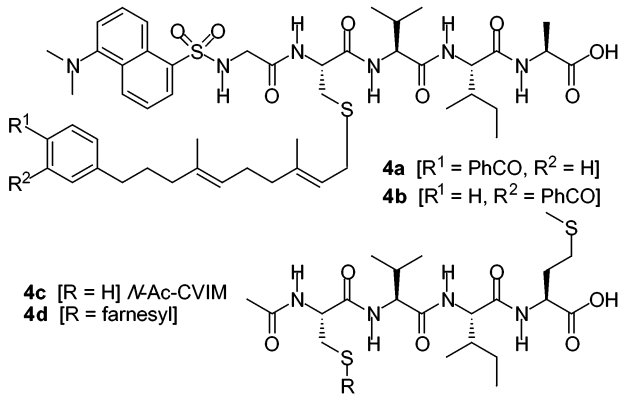

FIGURE 3: Expected products of reaction between **3a** or **3b** and Dn-GCVIA catalyzed by yPFTase prepared by chemical synthesis. The peptide substrate N-Ac-CVIM (**4c**) and its farnesylated product **4d** are also shown.

RESULTS

Substrate Studies. To determine whether **3a** and **3b** were substrates for yPFTase, a continuous fluorescence assay using the pentapeptide Ds-GCVIA was employed. This assay monitors the increase in fluorescence of the dansyl group upon prenylation at the neighboring cysteine residue caused by the change in hydrophobicity as previously described (*35*, *36*). No observable change in the fluorescence of the pentapeptide was observed in reactions containing **3a** or **3b** in place of FPP, which suggests that these compounds are not substrates for yPFTase. To further study this question, the expected products of the enzymatic prenylation of Ds-GCVIA with **3a** and **3b** were prepared by chemical synthesis using the method of Xue et al. (*32*) and are shown in Figure 3.

The chemically synthesized products were purified by reversed-phase HPLC and analyzed by ESI-MS and ESI-MS/MS to confirm their structure. For **4a**, an $[M + H]^+$ peak of 1041.2, an $[M + Na]^+$ peak of 1063.2, and an $[M + K]^+$ peak of 1079.2 were observed. Similar peaks and values were obtained for **4b**. The ESI-MS/MS shows b-type fragmentation as well as loss of the analogue and dansyl group during the fragmentation process (data not shown). This implies that the linkage between the analogue and the peptide is readily cleaved. With the authentic products characterized, the products from large-scale enzymatic reactions (10 mL) between **3a** or **3b**, Ds-GCVIA, and yPFTase were analyzed by HPLC and compared to the chemically synthesized products. The HPLC chromatograms monitored by UV and fluorescence detection are shown in Figure 4 for the reaction between **3a** and Ds-GCVIA with yPFTase.

Similar results were seen for Ds-GCVIA and **3b** by yPFTase (data not shown). In both cases, the yields of product formed were considerably less than 1% (see Figure 4B). Since these large-scale reactions were performed with 18-fold greater amounts of enzyme and allowed to react for 6-fold longer times than would be necessary to quantitatively convert a reaction containing FPP and Ds-GCVIA, it can be seen that **3a** and **3b** react much slower, if at all, than FPP and are hence not efficient substrates for yPFTase. These results are similar to those found for the C_{10} benzoylbenzoate ester analogues, **3c** and **3d**, previously described (*37*).

Enzyme Inhibition. To evaluate their potential as enzyme inhibitors, the rate of yPFTase-catalyzed farnesylation of a peptide substrate, Ds-GCVIA, was measured at fixed concentrations of FPP and varying concentrations of **3a** and **3b**. In the presence of natural substrate, **3a** and **3b** attenuated the rate of peptide prenylation, indicating that these compounds are enzyme inhibitors. Plots of $1/v$ versus [I] gave IC_{50} values of 1.4 ($\pm$0.18) μM for **3a** and 0.93 ($\pm$0.19) μM for **3b**. To examine the mechanism of inhibition in greater detail, the rate of yPFTase-catalyzed prenylation of Ds-GCVIA was measured in the presence of fixed concentrations of the isoprenoid substrate, FPP, and varying concentrations of **3a** and **3b**. Double reciprocal plots of these data for **3a** and **3b**, presented in Figure 5, both give patterns of lines that intersect on the $1/v$ axis, consistent with competitive inhibition with respect to the substrate FPP. Further kinetic experiments and analysis by the method of Eadie−Hofstee gave K_I values of 45 nM (**3a**) and 49 nM (**3b**) for yPFTase. These values are summarized in Table 1, together with those obtained with several related ester- and amide-based analogues, **3c**−**e** (*37*, *38*). Comparison of these values shows that the ether-linked compounds are 7−20-fold more potent inhibitors than the related carbonyl-containing progenitors. This may reflect a deleterious effect on binding due to the presence of the carbonyl groups present in **3c**−**e** or an effect of the more rigid ester and amide linkages to be accommodated into the isoprenoid binding pocket. The K_I values compiled in Table 1 were determined from kinetic analyses performed by varying the FPP concentration and holding the peptide concentration constant. Since the PFTase-catalyzed reaction proceeds via an ordered sequential mechanism where FPP binds first, the K_I values determined in this manner are independent of the peptide concentration and equal to the dissociation constant of the binary enzyme−inhibitor complex. Comparison of the K_I values for **3a** and **3b** with the K_D of 75 nM obtained for FPP by Dolence et al. (*39*) indicates that these analogues bind at least as well, if not more effectively, to yPFTase than the natural substrate; the presence of the benzoylbenzyl groups in **3a** and **3b** results in a ca. 1.5-fold increase in binding affinity for yPFTase

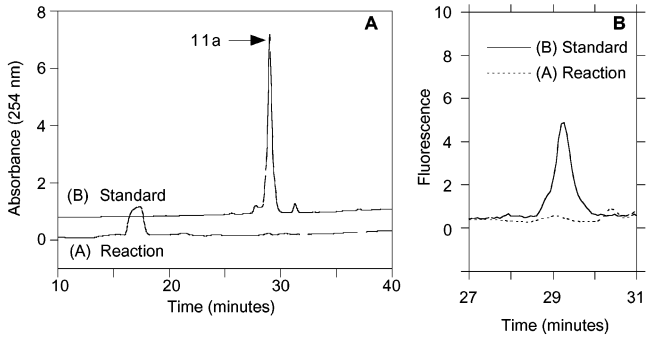

FIGURE 4: HPLC analysis of the reaction mixture containing **3a**, Dn-GCVIA, and yPFTase. Panel A: UV analysis. Chromatogram A is from a 10 mL reaction mixture containing Dn-GCVIA and **3a**. Chromatogram B is from a sample of chemically synthesized **4a**. The amount of **4a** injected is equal to the amount of product that would be formed in the enzymatic reaction assuming 100% conversion. Panel B: Fluorescence detection. Chromatogram A is from a 10 mL reaction mixture containing Dn-GCVIA and **3a**. Chromatogram B is from a sample of chemically synthesized **4a**. The amount of **4a** injected is equal to the amount of product that would be formed in the enzymatic reaction assuming 1% conversion. The broad peak at 17 min in chromatogram A is from **3a**, which decomposes on the column under the acidic separation conditions.

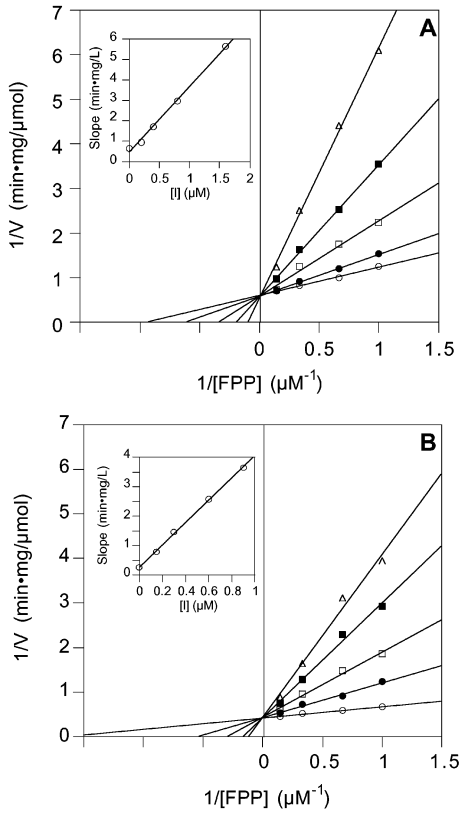

FIGURE 5: Double reciprocal plots showing the competitive inhibition of yPFTase with respect to FPP (**1**) by **3a** and **3b**. The concentrations of **3a** and **3b** are as follows: 0, 0.20, 0.40, 0.80, and 1.6 μM for **3a** and 0, 0.15, 0.30, 0.60, and 0.90 μM for **3b**. Inset: Replot of slopes from the double reciprocal plot versus [**3a**] or [**3b**]. Panel A: Inhibition by **3a**. Panel B: Inhibition by **3b**.

Table 1: Comparison of K_I Values Obtained for Benzophenone-Based Photoaffinity Analogues Using a C_{10} Isoprenoid Spacer Containing Ether, Ester, or Amide Linkages

compd	benzophenone linkage	benzophenone substitution	yPFTase K_I (nM)
3a	ether	para	45 ± 10
3b	ether	meta	49 ± 7
3c	ester	para	910[a]
3d	ester	meta	380[a]
3e	amide	meta	700[b]
FPP			75 (K_D)[c]

[a] From Gaon et al. (*37*). [b] From Turek et al. (*38*). [c] From Dolence et al. (*39*).

when compared to FPP. The kinetics of inhibition of yPFTase by **3b** in the presence of fixed concentrations of FPP and varying concentrations of the peptide substrate **4c** were also examined. Unfortunately, analysis of that data produced a complex inhibition pattern that was not easily interpretable. One reason for this is that yPFTase exhibits substrate inhibition at high concentrations of peptide due to the ordered nature of the kinetic mechanism.

Photoinactivation Studies. Photolysis reactions of yPFTase in the presence of **3a** or **3b** were performed by irradiating mixtures of these analogues and yPFTase, withdrawing aliquots at regular intervals, and assaying the resulting samples for residual activity. This resulted in 40% inactivation over 12 h for both analogues, comparable to results previously obtained with **3c** and **3d** (data not shown) (*37*). Significant inactivation did not occur upon irradiation in the absence of **3a** or **3b** and could be largely prevented by the simultaneous inclusion of FPP to displace the bound analogue.

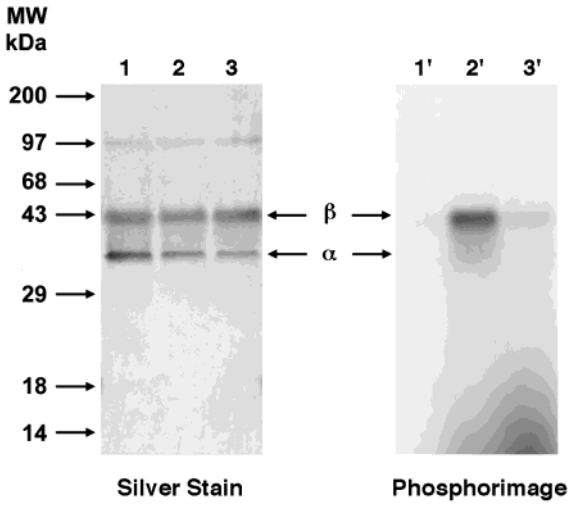

FIGURE 6: Photoaffinity labeling of yPFTase using [^{32}P]-**3b**. Electrophoretic analysis (SDS−PAGE) of reactions containing yPFTase and [^{32}P]-**3b**. Lanes 1 and 1′: yPFTase (2.9 μg, 380 nM) and [^{32}P]-**3b** (1.0 μM) without irradiation. Lanes 2 and 2′: yPFTase and [^{32}P]-**3b** after irradiation. Lanes 3 and 3′: yPFTase and [^{32}P]-**3b** after irradiation in the presence of FPP (**1**, 50 μM). Silver staining of the gel shown in lanes 1−3 illustrates the total protein present. Phosphorimaging of the gel shown in lanes 1′−3′ shows the associated radioactivity after irradiation.

Photolabeling of Protein Prenyl Transferases. To obtain structural information concerning the binding of **3a** and **3b** to yPFTase, photoaffinity labeling experiments were performed. Radioactive analogues [^{32}P]-**3a** and [^{32}P]-**3b** were synthesized as previously described (*33*, *37*). Irradiation of the enzyme at 350 nm for 2 h in the presence of [^{32}P]-**3b** (1 μM) resulted in preferential labeling of the β subunit as shown in Figure 6 (lane 2′). Inclusion of the natural substrate, FPP, resulted in protection from labeling (Figure 6, lane 3′). Similar results were obtained with 1.0 μM [^{32}P]-**3a** (data not shown). To quantitate the relative labeling efficiencies of each subunit for each reaction, a phosphorimager apparatus was employed (data not shown). For photolabeling of yPFTase with [^{32}P]-**3a**, the β subunit was labeled 4.2-fold over the α subunit. Addition of FPP in the photolysis reaction resulted in a 5.5-fold decrease in β subunit labeling and a 1.3-fold decrease in α subunit labeling. Similar experiments with [^{32}P]-**3b** resulted in labeling of the β subunit 4.5-fold over the α subunit with a 8.5-fold decrease in β subunit labeling and a 1.6-fold decrease in α subunit labeling upon addition of FPP. Compared to our earlier work with ester- and amide-linked benzophenone analogues, **3b** appears to exhibit the highest preference for labeling of the β subunit over the α subunit. Moreover, the fold reduction in labeling of yPFTase in the presence of saturating concentrations of FPP was significantly higher with **3b** than with the previously reported ester- and amide-linked homologues; thus, the ether-linked probe **3b** appears to be the most specific photoactive FPP analogue we have prepared to date. Finally, photolabeling experiments similar to those described above were also performed with hPFTase and gave comparable results. Taken together, the above results suggest that the β subunit is involved in prenyl diphosphate recognition for yPFTase and hPFTase, consistent with previous photolabeling work

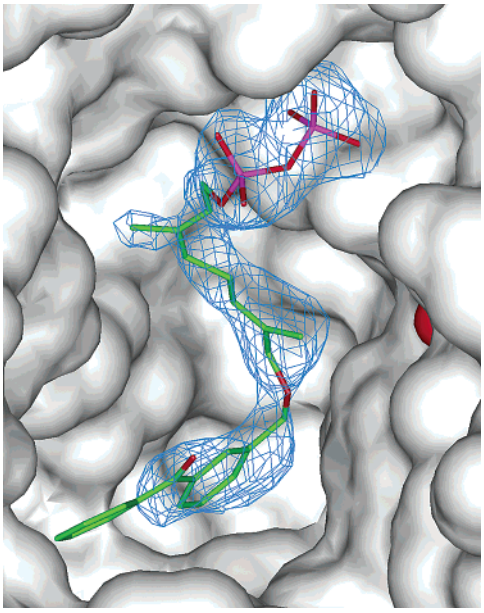

FIGURE 7: Structure of **3b** bound to rPFTase as determined by X-ray analysis. $2F_o - F_c$ electron density contoured at 1σ for **3b** is shown in blue. The solvent-accessible protein surface is white with the Zn atom shown in red.

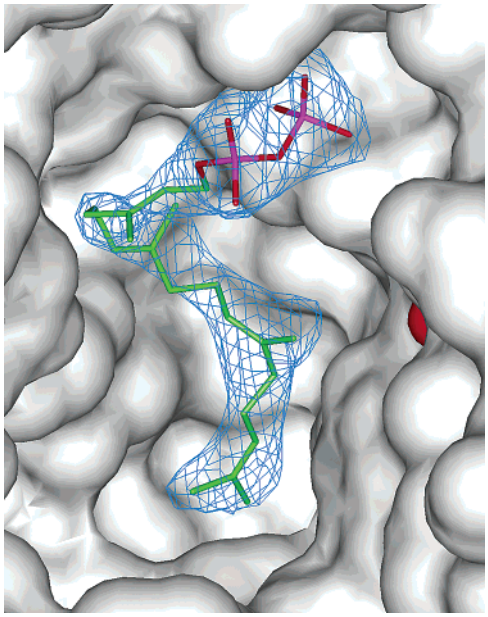

FIGURE 8: Structure of GGPP (**2**) bound to rPFTase as determined by X-ray analysis. $2F_o - F_c$ electron density contoured at 1σ for the GGPP is shown in blue. The solvent-accessible protein surface is white with the Zn atom shown in red.

from our laboratory and others (*29*, *37*, *38*, *40*−*43*). Such a model is also consistent with high-resolution structural studies performed with the related rPFTase (*23*, *24*, *26*−*29*).

*Structural Analysis of **3b** Bound to rPFTase.* To gain insight into why these isoprenoid diphosphate analogues apparently bind to PFTase but are not turned over, crystals of **3b** bound to rPFTase were obtained, and the structure of the resulting complex was determined via X-ray diffraction experiments. Electron density maps (see Figure 7) clearly show the bound conformation and location of **3b** in the PFTase active site cavity although there is no electron density for the distal ring of the benzophenone moiety. The presence of the higher molecular weight phosphate atoms in the molecule assists in unambiguous definition of the binding mode although there is a gradual increase in the crystallographic *B* factors from 30 to 60 Å^2 in going from the phosphates to the benzophenone carbonyl unit. The distal ring is probably not visible since it projects into an open region (the peptide binding site; see below) where its movement is unconstrained by the protein although the proximal ring and carbonyl are clearly visible and located within 4 Å of W102β, R202β, Y205β, C206β, and C254β.

Comparison of the protein in the structure of the PFTase·**3b** complex and the PFTase·FPP·SCH66336 ternary complex shows a 0.2 Å rms deviation for all protein atoms, indicating minimal movement of protein side chains (*26*, *27*). The positions of the diphosphate atoms and the first and second isoprene units are well conserved between **3b** and FPP while the benzophenone group extends past the binding site of the third isoprene unit deeper into the PFTase active site. Comparison of the structures of the binary PFTase·**3b** complex with the ternary PFTase·HFP·CVIM complex shows that the benzophenone moiety projects into the binding pocket occupied by the C-terminal substrate-derived methionine residue. Thus it appears that the PFTase active site cannot simultaneously accommodate **3b** and the protein substrate. Binding of the prenyl diphosphate analogue physically occludes peptide substrate binding, which in turn prevents subsequent catalytic turnover despite the fact that the C-1 position and the diphosphate moiety are located at the same positions as the corresponding atoms in FPP.

Structural Analysis of GGPP Bound to rPFTase. To examine whether the binding of longer isoprenoidal compounds to PFTase occurs only via extension into the peptide site, we sought to obtain a structure containing a different prenyl diphosphate. Crystals containing GGPP (**2**) bound to PFTase were used to determine the structure via X-ray diffraction experiments. Electron density maps provide clear information regarding the conformation and location of GGPP in the PFTase active site cavity (Figure 8). A superposition of GGPP, **3b**, and FPP in the isoprenoid binding pocket of rPFTase is shown in Figure 9. As was seen in the PFTase·**3b** structure, comparison of the protein in the structure of the PFTase·GGPP complex and the PFTase·FPP·SCH66336 ternary complex shows minimal movement of protein side chains. Similar to the PFTase·**3b** structure, the positions of the diphosphate atoms are well conserved between GGPP and FPP. However, in contrast to the PFTase·**3b** complex, the first and second isoprene units of the bound GGPP molecule are reoriented, bulging away from the protein substrate binding site into an unoccupied region. The first isoprenoid unit lies within 4 Å of K164α, Y200α, and H201α, and the second unit is located within 4 Å of Y166α, H248β, and Y251β. The third and fourth isoprene units are located in the position occupied by the second and third isoprene groups of FPP. Thus, unlike **3b**, the binding of GGPP does not block the binding of the peptide substrate. Therefore, some other mechanism underlies the lack of catalysis.

Structural Analysis of the Farnesylated CVIM Peptide Bound to rPFTase. The structure of a CVIM peptide and a FPP analogue bound to rPFTase has been previously described (*26*). Given the large distance (ca. 7 Å) between

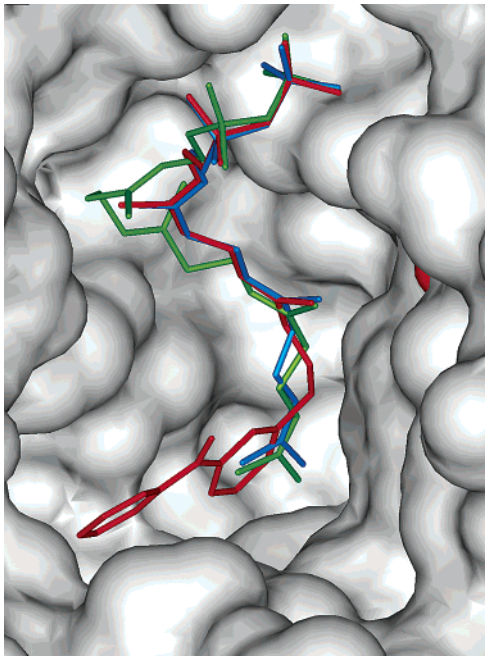

FIGURE 9: Superposition of the structures of isoprenoids bound to rPFTase. Compounds are **3b** (red), GGPP (green), and FPP (blue). The solvent-accessible protein surface is white with the Zn atom shown in red.

the peptide-derived sulfur nucleophile and the C-1 position of the isoprenoid in that structure, it was clear that either the peptide or isoprenoid substrate would have to move in order for catalysis to occur. To clarify the uncertainty of what moves and to understand the mechanism of inhibition by GGPP, the structure of the farnesylated CVIM product (**4d**) was obtained. Cocrystals of rPFTase grown in the presence of both *N*-acetyl-CVIM and FPP were used to determine the structure via X-ray diffraction experiments. During crystal growth the two substrates were converted to product as there is clear electron density for the bound product. The structure of farnesylated CVIM bound to PFTase is shown in Figure 10.

Comparison of the protein in the product structure complex and the **3b** and GGPP structures shows minimal differences in the protein conformation. The diphosphate group is not visible in the electron density map and has presumably diffused out of the active site. As suggested by biophysical measurement, the cysteine sulfur remains coordinated to the zinc after product formation (*44*−*46*). The conformation of the peptide portion of the product is similar to the substrate peptide structure. Interestingly, there is a major change in the conformation of the prenyl group (Figure 10). The third isoprenoid unit of the farnesyl portion of the product (shown in red) is unchanged compared to the bound FPP (shown in blue). However, there is a 180° rotation of the second isoprenoid unit and a similar rotation of the first isoprenoid unit so that the C-1 carbon can form a bond with the cysteine of the peptide; note that C-1 of the isoprenoid is highlighted by a blue ball in FPP and by a red ball in the product structures superimposed in Figure 10. Thus, it is clear that, during catalysis, it is the isoprenoid substrate that is in motion and not the peptide. Whether that motion is coupled to protein movements that occur en route to the transition state or not remains unknown.

DISCUSSION

The results described here demonstrate that prenyl diphosphate analogues **3a** and **3b** bind to PFTase with high affinity to the isoprenoid binding site but are not processed catalytically by the enzyme. Previously, it had been reported that GGPP manifested similar properties (*21*, *22*). The structural analysis presented here shows that both **3b** and GGPP bind to the isoprenoid binding site of PFTase with the diphosphate group and the C-1 carbon occupying similar positions as the corresponding atoms in enzyme-bound FPP. This is different

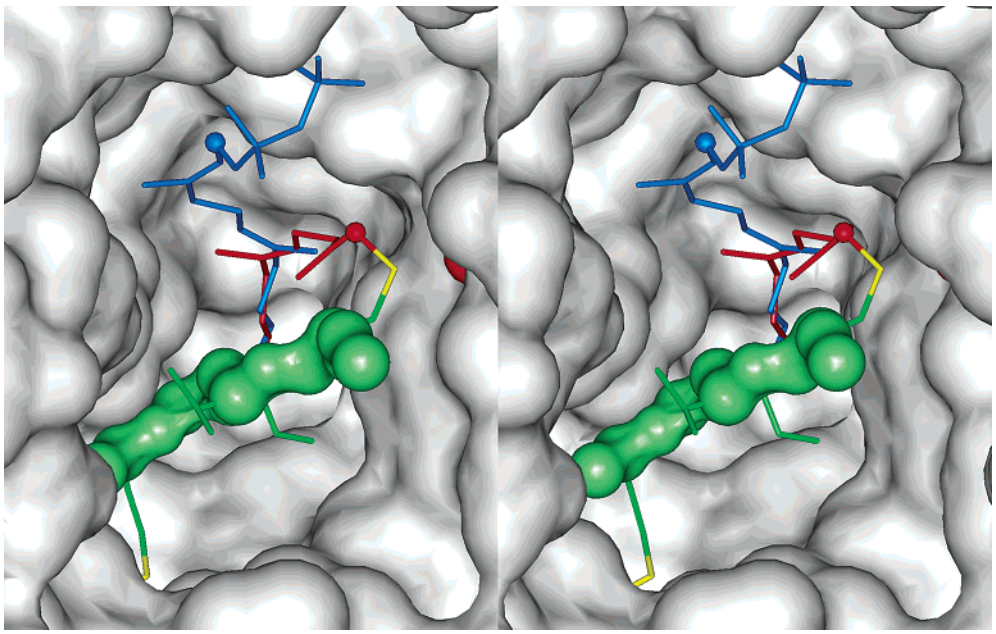

FIGURE 10: Stereo representation of farnesylated CVIM (**4d**) bound to rPFTase. The peptide portion is shown in green with the backbone atoms highlighted in a space-filling representation and the isoprenoid colored red. The structure of FPP from the binary FPP·rPFTase complex (blue) is superimposed to show how the isoprenoid moves during the enzyme-catalyzed reaction. The C-1 position of the isoprenoid is highlighted as a blue ball in the binary FPP·rPFTase complex and as a red ball in the product complex. The solvent-accessible protein surface is white with the Zn atom shown in red.

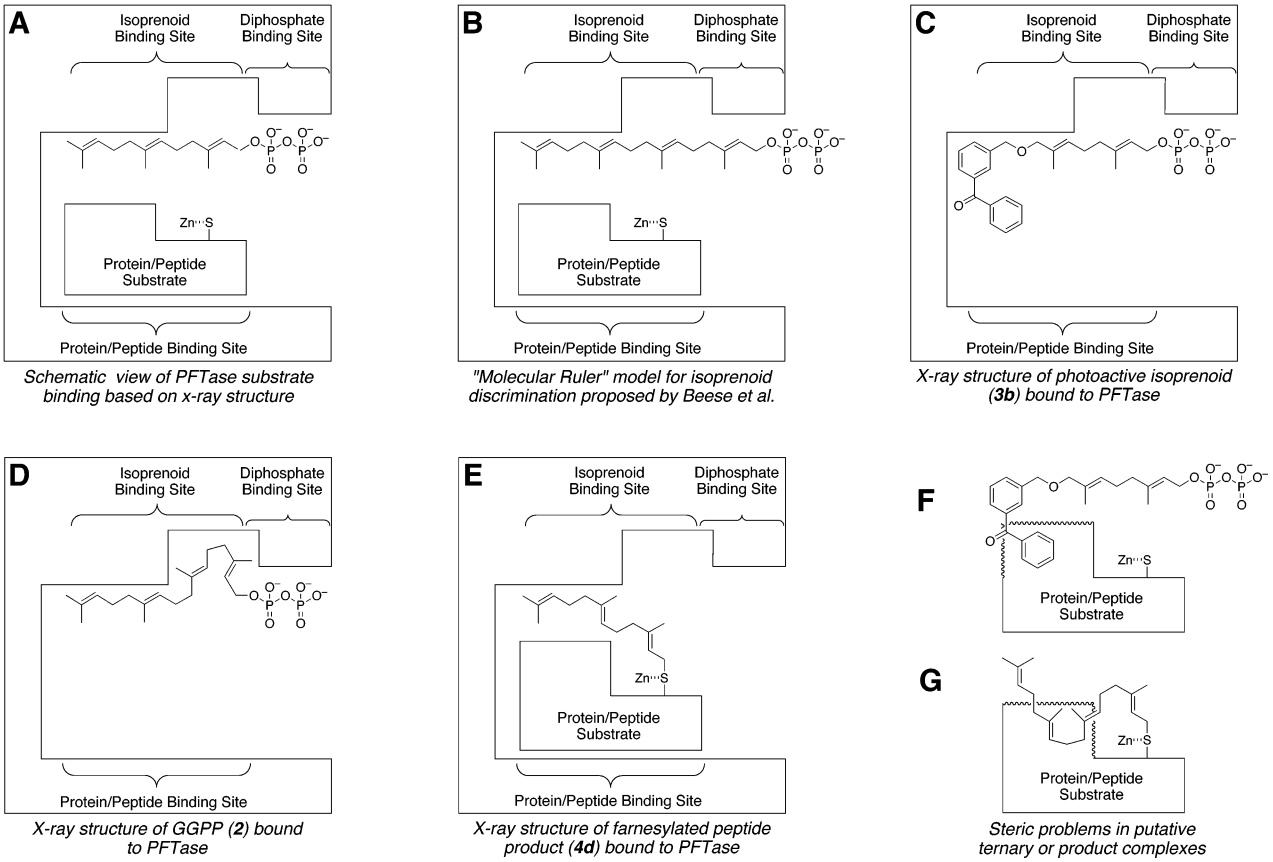

FIGURE 11: Schematic representations of the molecular ruler hypothesis and proposed second site exclusion model for how PFTase discriminates between FPP, GGPP, and other isoprenoid analogues.

than what was predicted by the molecular ruler hypothesis as described by Beese and co-workers (*24*). In that model, it was hypothesized that isoprenoid binding would be constrained by the depth of the prenyl binding site. Larger, noncognate prenyl diphosphates would bind, filling up the isoprenoid pocket and leaving the diphosphate and first isoprenoid unit incorrectly positioned for efficient catalysis; this is shown schematically in Figure 11B.

However, as noted above, the diphosphates in the structures of both **3b** and GGPP are not displaced in this fashion. Instead, they map to positions that are indistinguishable from those of FPP, as illustrated in Figure 9. In both cases, it is the isoprenoid that is conformationally perturbed.

Interestingly, one consequence of this perturbation is that the larger isoprenoids bulge into pockets in the active site. In the case of **3b**, the isoprenoid occupies part of the CVIM substrate binding site and, in doing so, would prevent its binding and subsequent reaction (Figure 11C,F). In the case of GGPP, the situation is somewhat different. In order for the enzyme to incorporate this substrate, the C-1 position must move in a fashion analogous to the same position in FPP to produce a product complex similar to that shown in Figure 11E. As this occurs, steric clashes (see Figure 11G) with the peptide substrate would ensue. Thus, it appears that the prenyl diphosphate substrate specificity of PFTase is controlled, not by misalignment of the diphosphate moiety but through the subsequent binding of the protein substrate. In the case of **3a**, it is the formation of the ternary complex that is inhibited, while with GGPP it is the subsequent conversion of the ternary complex to the product that is prevented. Here, we propose that this "second site exclusion model" provides a better explanation for how PFTase discriminates against larger isoprenoid substrates. It is also interesting to note that this model predicts the importance of the diphosphate unit as a major contributor to the binding energy of prenyl diphosphate analogues. The allylic alcohol precursors to **3a** and **3b** that lack the diphosphate moiety are not effective inhibitors of PFTase. This latter observation would not have been predicted by the molecular ruler hypothesis.

Taken together, the results reported here, codified in this second site exclusion model, provide a clear picture of how PFTase discriminates between FPP and larger isoprenoidal substrates. In addition, the structural data described here may provide new insights for inhibitor design. Since it is clear that PFTase can tolerate a number of modifications in the third isoprene unit, it may be possible to introduce additional functionality at that position beyond the benzophenone photophore that will substantially augment the potency of such prenyl diphosphate analogues. The alternative conformation of the farnesyl group in the product complex suggests that PFTase may also accommodate modifications in the first and second isoprenoid units. This greatly increases the possible repertoire of inhibitors based on the prenyl diphosphate substrate that could be designed. Such compounds would bear little structural resemblance to current PFTase inhibitors and could have new and useful properties.

NOTE ADDED IN PROOF

Recently, the structure of a related farnesylated peptide bound to PFTase was reported (*47*). That structure is

essentially the same as that of the **4d**·PFTase complex described here.

ACKNOWLEDGMENT

The authors thank Dr. Leo Bonilla and Nancy Raha, University of Minnesota Cancer Institute, for obtaining the mass spectral data.

REFERENCES

1. Casey, P. J., Solski, P. A., Der, C. J., and Buss, J. E. (1989) *Proc. Natl. Acad. Sci. U.S.A. 86*, 8323−8327.
2. Schafer, W. R., Trueblood, C. E., Yang, C.-C., Mayer, M. P., Rosenberg, S., Poulter, C. D., Kim, S.-H., and Rine, J. (1990) *Science 249*, 1133−1139.
3. Goodman, L. E., Judd, S. R., Farnsworth, C. C., Powers, S., Gelb, M. H., Glomset, J. A., and Tamanoi, F. (1990) *Proc. Natl. Acad. Sci. U.S.A. 87*, 9665−9669.
4. Schaber, M. D., O'Hara, M. B., Garsky, V. M., Mosser, S. D., Bergstrom, J. D., Moores, S. L., Marshall, M. S., Friedman, P. A., Dixon, R. A., and Gibbs, J. B. (1990) *J. Biol. Chem. 265*, 14701−14704.
5. Manne, V., Roberts, D., Tobin, A., O'Rourke, E., De Virgilo, M., Meyers, C., Ahmed, N., Kurz, B., Resh, M., Kung, H.-F., and Barbacid, M. (1990) *Proc. Natl. Acad. Sci. U.S.A. 87*, 7541−7545.
6. Casey, P. J., Thissen, J. A., and Moomaw, J. F. (1991) *Proc. Natl. Acad. Sci. U.S.A. 88*, 8631−8635.
7. Zhang, F. L., and Casey, P. J. (1996) *Annu. Rev. Biochem. 65*, 241−269.
8. Schafer, W. R., and Rine, J. (1992) *Annu. Rev. Genet. 30*, 209−237.
9. Reiss, Y., Goldstein, J. L., Seabra, M. C., Cassey, P. J., and Brown, M. S. (1990) *Cell 62*, 81−88.
10. Kohl, N. E., Mosser, S. D., deSolms, S. J., Giuliani, E. A., Pompliano, D. L., Graham, S. L., Smith, R. L., Scolnick, E. M., Oliff, A., and Gibbs, J. B. (1993) *Science 260*, 1934−1937.
11. Nigam, M., Seong, C.-M., Qian, Y., Hamilton, A. D., and Sebti, S. M. (1993) *J. Biol. Chem. 268*, 20695−20698.
12. Nagasu, T., Yoshimatsu, K., Rowell, C., Lewis, M. L., and Garcia, A. M. (1995) *Cancer Res. 55*, 5310−5314.
13. Sepp-Lorenzino, L., Ma, Z., Rands, E., Kohl, N. E., Gibbs, J. B., Oliff, A., and Rosen, N. (1995) *Cancer Res. 55*, 5302−5309.
14. Karp, J. E., Kaufmann, S. H., Adjei, A. A., Lancet, J. E., Wright, J. J., and End, D. W. (2001) *Curr. Opin. Oncol. 13*, 470−476.
15. Britten, C. D., Rowinsky, E. K., Soignet, S., Patnaik, A., Yao, S. L., Deutsch, P., Lee, Y., Lobell, R. B., Mazina, K. E., McCreery, H., Pezzuli, S., and Spriggs, D. (2001) *Clin. Cancer Res. 7*, 3894−3903.
16. Zujewski, J., Horak, I. D., Bol, C. J., Woestenborghs, R., Bowden, C., End, D. W., Piotrovsky, V. K., Chiao, J., Belly, R. T., Todd, A., Kopp, W. C., Kohler, D. R., Chow, C., Noone, M., Hakim, F. T., Larkin, G., Gress, R. E., Nussenblatt, R. B., Kremer, A. B., and Cowan, K. H. (2000) *J. Clin. Oncol. 18*, 927−941.
17. Patnaik, A., and Rowinsky, E. K. (2001) *Farnesyltransferase Inhibitors in Cancer Therapy*, pp 233−249.
18. Adjei, A. A., Erlichman, C., Davis, J. N., Cutler, D. L., Sloan, J. A., Marks, R. S., Hanson, L. J., Svingen, P. A., Atherton, P., Bishop, W. R., Kirschmeier, P., and Kaufmann, S. H. (2000) *Cancer Res. 60*, 1871−1877.
19. Sebti, S. M., and Hamilton, A. D. (2000) *Oncogene 19*, 6584−6593.
20. Reiss, Y., Stradley, S. J., Gierasch, L. M., Brown, M. S., and Goldstein, J. L. (1991) *Proc. Natl. Acad. Sci. U.S.A. 88*, 732−736.
21. Casey, P. J., and Seabra, M. C. (1996) *J. Biol. Chem. 271*, 5289−5292.
22. Reiss, Y., Brown, M. S., and Goldstein, J. L. (1992) *J. Biol. Chem. 267*, 6403−6408.
23. Park, H.-W., Boduluri, S. R., Moomaw, J. F., Casey, P. J., and Beese, L. S. (1997) *Science 275*, 1800−1804.
24. Long, S. B., Casey, P. J., and Beese, L. S. (1998) *Biochemistry 37*, 9612−9618.
25. Dunten, P., Kammlott, U., Crowther, R., Weber, D., Palermo, R., and Birktoft, J. (1998) *Biochemistry 37*, 7907−7912.
26. Strickland, C. L., Windsor, W. T., Syto, R., Wang, L., Bond, R., Wu, Z., Schwartz, J., Le, H. V., Beese, L. S., and Weber, P. C. (1998) *Biochemistry 37*, 16601−16611.
27. Strickland, C. L., Weber, P. C., Windsor, W. T., Wu, Z., Le, H. V., Albanese, M. M., Alvarez, C. S., Cesarz, D., Rosario, J. D., Deskus, J., Mallams, A. K., Njoroge, F. G., Piwinski, J. J., Remiszewski, S., Rossman, R. R., Taveras, A. G., Vibulbhan, B., Doll, R. J., Girijavallabhan, V. M., and Ganguly, A. K. (1999) *J. Med. Chem. 42*, 2125−2135.
28. Long, S. B., Casey, P. J., and Beese, L. S. (2000) *Structure 8*, 209−222.
29. Turek, T. C., Gaon, I., Distefano, M. D., and Strickland, C. L. (2001) *J. Org. Chem. 66*, 3253−3264.
30. Long, S. B., Hancock, P. J., Kral, A. M., Hellinga, H. W., and Beese, L. S. (2001) *Proc. Natl. Acad. Sci. U.S.A. 98*, 12948−12953.
31. Gaon, I., Turek, T. C., and Distefano, M. D. (1996) *Tetrahedron Lett. 37*, 8833−8836.
32. Xue, C.-B., Becker, J. M., and Naider, F. (1992) *Tetrahedron Lett. 33*, 1435−1438.
33. Turek, T. C., Gaon, I., and Distefano, M. D. (1997) *J. Labelled Compd. Radiopharm. 39*, 140−146.
34. Adamson, P., Marshall, C. J., Hall, A., and Tilbrook, P. A. (1992) *J. Biol. Chem. 267*, 20033−20038.
35. Pompliano, D. L., Gomez, R. P., and Anthony, N. J. (1992) *J. Am. Chem. Soc. 114*, 7945−7946.
36. Bond, P. D., Dolence, J. M., and Poulter, C. D. (1995) *Methods Enzymol. 250*, 30−43.
37. Gaon, I., Turek, T. C., Weller, V. A., Edelstein, R. L., Singh, S. K., and Distefano, M. D. (1996) *J. Org. Chem. 61*, 7738−7745.
38. Turek, T. C., Gaon, I., Gamache, D., and Distefano, M. D. (1997) *Bioorg. Med. Chem. Lett. 7*, 2125−2130.
39. Dolence, J. M., Cassidy, P. B., Mathis, J. R., and Poulter, C. D. (1995) *Biochemistry 34*, 16687−16694.
40. Turek, T. C., Gaon, I., and Distefano, M. D. (1996) *Tetrahedron Lett. 37*, 4845−4848.
41. Edelstein, R. L., and Distefano, M. D. (1997) *Biochem. Biophys. Res. Commun. 235*, 377−382.
42. Bikhtiyarov, Y. E., Omer, C. A., and Allen, C. M. (1995) *J. Biol. Chem. 270*, 19035−19040.
43. Yokoyama, K., McGeady, P., and Gelb, M. H. (1995) *Biochemistry 34*, 1344−1354.
44. Huang, C.-C., Casey, P. J., and Fierke, C. A. (1997) *J. Biol. Chem. 272*, 20−23.
45. Rozema, D. B., and Poulter, C. D. (1999) *Biochemistry 38*, 13138−13146.
46. Huang, C.-C., Hightower, K. E., and Fierke, C. A. (2000) *Biochemistry 39*, 2593−2602.
47. Long, S. B., Casey, P. J., and Beese, L. S. (2002) *Nature 419*, 645−650.

BI0266838